https://doi.org/10.15407/ujpe71.5.469

M. ZEBACH, A. HEMMANI, H. KHACHAB

Laboratory for the Development of Renewable Energies
and their Applications in Saharan Areas,
TAHRI Mohammed University, Bechar-Algeria 08000
(P.O. Box 417 Qanadsa Road, Bechar, Algeria)

PERFORMANCE OPTIMISATION OF BIFACIAL CZTS THIN-FILM SOLAR CELLS TO ACHIEVE MAXIMUM POWER CONVERSION EFFICIENCY

Kesterite Cu_2ZnSnS_4 (CZTS) is among the most promising absorber materials for thin-film solar cells due to its direct bandgap (1.1–1.5 eV), high absorption coefficient ($>10^4$ cm^{-1}), earth abundance, non-toxicity, and low production cost. Despite these advantages, the efficiency of CZTS-based devices remains limited by secondary phase formation, electronic defects, and fabrication instability. In this work, a numerical model for a bifacial CZTS thin-film solar cell is developed using a self-consistent Poisson–drift–diffusion framework implemented in MATLAB/Simulink. By optimising the absorber and buffer layer thicknesses, a maximum power conversion efficiency (PCE) of 19.66% is achieved for a bifacial CZTS device with a 4 μm absorber and a 10 nm CdS buffer layer. This result exceeds reported experimental efficiencies for comparable CZTS heterojunctions (approximately 15.8%) while remaining below the Shockley–Queisser theoretical limit of 32.4%. The findings highlight the potential of bifacial CZTS architectures as an effective strategy for enhancing photovoltaic performance.

Keywords: CZTS solar cells, thin films, bifacial photovoltaics, numerical simulation, heterojunction.

1. Introduction

Thin-film photovoltaic technologies mainly depend on amorphous silicon (a-Si), which reaches efficiencies of about 14%, and cadmium telluride (CdTe), which has achieved record power conversion efficiencies of 23.1%. Copper indium gallium diselenide (CIGS) solar cells have also attained a record efficiency of 23.6% [1]. However, further large-scale development of these leading absorber materials is limited by material availability and environmental issues: Cd is toxic and classified as a heavy metal, Te is rare, and In and Ga are both scarce in supply and costly [2–5]. These challenges have spurred the search for eco-friendly absorbers made from earth-abundant elements.

Among the most promising alternatives is the kesterite compound Cu_2ZnSnS_4 (CZTS), a non-toxic, earth-abundant absorber well suited for thin-film photovoltaics. CZTS offers favourable optoelectronic properties, including a high absorption coefficient ($>10^4$ cm^{-1}), a tunable bandgap in the 1.1–1.55 eV range, and a theoretical efficiency limit of 32.4% under the Shockley–Queisser framework [6]. Expe-

Citation: Zebach M., Hemmani A., Khachab H. Performance optimisation of bifacial CZTS thin-film solar cells to achieve maximum power conversion efficiency. *Ukr. J. Phys.* **71**, No. 5, 469 (2026). https://doi.org/10.15407/ujpe71.5.469.

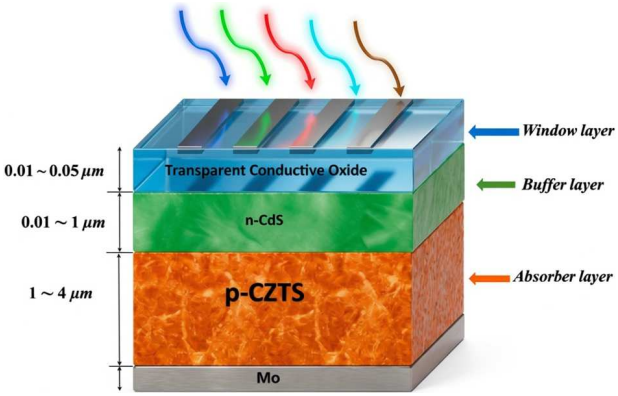

Fig. 1. Monofacial CZTS thin-film solar cell architectures

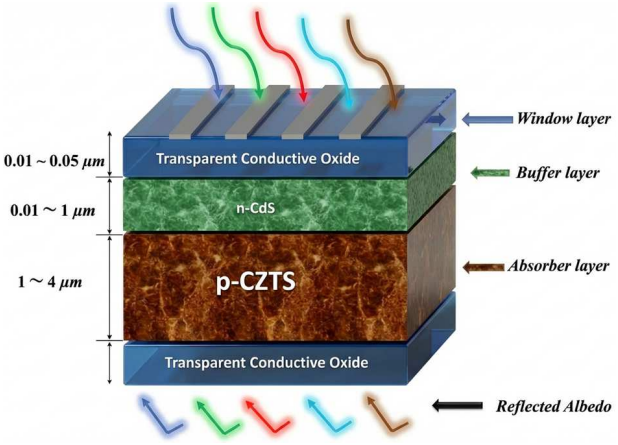

Fig. 2. Bifacial CZTS thin-film solar cell architectures

rimentally, CZTS devices fabricated on molybdenum (Mo) substrates have achieved efficiencies up to ∼12.6% using hydrazine-based pure-solution processing [7]. Despite this progress, CZTS performance remains far below that of commercial CIGS devices (∼21.6%), indicating significant room for improvement.

Conventional CZTS cells use an opaque Mo back contact, so illumination is limited to the front side. A practical way to improve energy yield is to adopt bifacial architectures, where the Mo layer is replaced by a transparent conductive oxide (TCO) such as fluorine-doped tin oxide (FTO), indium tin oxide (ITO), or molybdenum-doped indium oxide (MIO). This change allows for simultaneous front- and rear-side illumination, boosting overall photocurrent generation [8, 9]. Numerical modelling tools have been employed to optimise thin-film solar cell designs by maintaining the continuity of the electrostatic potential and solving the coupled Poisson and carrier-transport equations [10].

In this study, we utilise MATLAB/Simulink to accurately solve these governing equations and to evaluate the performance of bifacial CZTS devices. The optimised model attains a power conversion efficiency of 19.66% for a bifacial CZTS cell, marking the largest improvement among the tested configurations. This simulated efficiency considerably surpasses current laboratory records (∼15.1%) and approaches the theoretical maximum efficiency of CZTS absorbers (32.4%), highlighting the potential of bifacial CZTS designs for next-generation thin-film photovoltaics.

2. CZTS Monofacial and Bifacial Thin-Film Solar Cell Architectures

The present study is intended to deliver a comprehensive academic analysis of two CZTS thin-film solar-cell architectures, as shown in Figures 1 and 2, namely monofacial and bifacial configurations, by examining how their structural configurations govern power conversion efficiency. In the monofacial device, the conventional substrate configuration Mo/p-CZTS/n-CdS/TCO/metal grid is retained, where illumination is restricted to the front side through the transparent conductive oxide and CdS buffer. In this configuration, the molybdenum back contact functions as an efficient ohmic extractor for holes, thereby providing optical opacity. This results in the effective loss of photons not absorbed within the CZTS layer through rear-side transmission.

Consequently, monofacial operation depends entirely on front-incident photon harvesting and is strongly influenced by parasitic absorption in CdS at short wavelengths, reflection at the air/TCO and TCO/CdS interfaces, and recombination at the CZTS/CdS heterointerface. The p-type CZTS absorber, typically in the 1–4 μm range, serves as the dominant light-absorbing region, and its thickness must be optimised to ensure high photogeneration while limiting bulk recombination associated with intrinsic defects in kesterite. The n-type CdS buffer, which is typically tens of nanometres thick in practical devices, forms the p–n heterojunction, provides favourable conduction-band alignment for electron extraction, and passivates interface states.

However, it also introduces optical penalties when thickened, due to increased parasitic absorption and possible transport resistance. The TCO window layer must be maintained at an optimal thickness, ensuring both the maximisation of transmission and the maintenance of low sheet resistance for lateral electron collection to the front grid. In contrast, the bifacial CZTS device modifies this baseline architecture by replacing the opaque Mo rear electrode with a transparent conductive oxide, yielding a symmetric, optically accessible stack of TCO/n-CdS/p-CZTS/TCO. This structural alteration facilitates dual-sided illumination, thereby enabling the cell to harvest not only direct front light but also rear-incident photons emanating from reflected albedo. In the context of bifacial operation, rear photons enter through the back TCO and propagate through the CZTS absorber, and contribute to carrier generation in closer proximity to the rear interface. Consequently, the absorber must support effective carrier collection to ensure the proper management of nonuniform generation profiles that span both sides of the junction. While the fundamental heterojunction remains CdS/CZTS, bifacial devices impose stricter requirements on interface and contact engineering because the rear TCO simultaneously functions as an optical window and an electrical contact. Increases in rear interfacial recombination, imperfect band alignment, or elevated contact resistance have been shown to disproportionately suppress the rear response and reduce bifacial gain.

Optically, bifacial performance is determined by absorber thickness: excessively thin CZTS layers transmit a larger fraction of rear-incident photons without absorption, whereas thicker absorbers enhance rear harvesting but may intensify bulk recombination if defect management is inadequate. Consequently, bifacial design introduces a coupled optimisation among CdS thickness, CZTS thickness, and dual-TCO transparency/resistance, extending beyond the requirements for monofacial cells.

A comparative analysis of these architectures reveals that monofacial CZTS cells typically exhibit higher efficiency under standard front-side illumination, attributable to the superior electrical quality of Mo contacts and the optical confinement associated with an opaque back electrode. However, bifacial CZTS cells offer a pathway to higher real-world energy yield by exploiting rear illumination, particularly in high-albedo environments, provided that rear optical access and carrier extraction are carefully optimised. Therefore, analysis of both structures in parallel clarifies the distinct loss mechanisms, thickness trade-offs, and junction constraints that control CZTS device performance. This provides a rational basis for advancing earth-abundant kesterite photovoltaics towards more efficient and application-relevant bifacial configurations.

3. Simulation of Physical and Electrical Material Parameters

The electrical behaviour of the thin-film heterojunction solar cell is governed by a coupled set of semiconductor transport equations. According to Poisson's equation (see Eq. (1)), the spatial curvature of the electrostatic potential, denoted by ψ, is directly proportional to the net charge density q within the device. This includes free carriers (electrons, n, and holes, p), ionised donors (N_D^+), ionised acceptors (N_A^-), and defect-related charge (ρ_{def}). The following equation is employed to determine the internal electric field distribution that drives carrier separation.

The carrier continuity equations (see Eqs. (2) and (3)) enforce charge conservation by balancing the time variation of electron and hole densities with current divergence, optical generation G, and recombination losses R_n and R_p. When considered in conjunction with the drift–diffusion current relations (see Eqs. (4) and (5)), these equations form a self-consistent model that describes the generation, transportation, and collection of carriers across the heterojunction. The spatial profiles of potential and carrier concentrations can be computed by solving Poisson's equation in conjunction with the electron and hole continuity equations in MATLAB. This process enables the extraction of key electrical characteristics, such as the photovoltaic conversion efficiency (PCE), of a thin-film solar cell

$$\frac{\partial^2\psi}{\partial x^2} = -\frac{q}{\varepsilon_0\varepsilon_r}\left(p - n + N_D^+ - N_A^- + \frac{\rho_{\text{def}}}{q}\right), \tag{1}$$

$$\frac{\partial n}{\partial t} = -\frac{1}{q}\frac{\partial J_n}{\partial x} + G - R_n, \tag{2}$$

$$\frac{\partial p}{\partial t} = \frac{1}{q}\frac{\partial J_p}{\partial x} + G - R_p. \tag{3}$$

The charge carrier transport, as governed by drift and diffusion mechanisms, is described by the following

Table 1. **Basic parameters used in the simulation of CZTS-based solar cells**

Layer properties	TCO	CdS	CZTS
Layer thickness w (μm)	$0.01 \sim 0.05$	$0.01 \sim 1$	$3 \sim 4$
Electron affinity χ (eV)	4.35	4.3	4.1
Relative permittivity ε_r	9	9	13.6
Electron mobility μ_n ($\mathrm{cm}^2/\mathrm{V\,s}$)	100	100	100
Hole mobility μ_p ($\mathrm{cm}^2/\mathrm{V\,s}$)	25	25	25
Donor concentration N_D (cm^{-3})	1×10^{18}	1.1×10^{18}	–
Acceptor concentration N_A (cm^{-3})	–	–	1×10^{17}
Band gap energy E_g (eV)	3.3	2.4	1.5
Effective conduction band density of states N_c (cm^{-3})	2.2×10^{18}	1.8×10^{19}	2.2×10^{18}
Effective valence band density of states N_v (cm^{-3})	1×10^{19}	2.4×10^{18}	1.8×10^{19}
Hole recombination velocity at CdS front surface S_p (cm/s)	10^7	10^7	–
Electron recombination velocity at CZTS back surface S_n (cm/s)	–	–	10^7
Defect density N_t (cm^{-3})	–	1×10^{17}	1×10^{16}
Electron capture cross section σ_e (cm^2)	–	10^{-12}	10^{-14}
Hole capture cross section σ_h (cm^2)	–	10^{-15}	10^{-15}

equations:

$$J_n = -q\mu_n \frac{\partial \psi}{\partial x} + qD_n \frac{\partial n}{\partial x}, \tag{4}$$

$$J_p = -qD_p \frac{\partial p}{\partial x} - q\mu_p \frac{\partial \psi}{\partial x}. \tag{5}$$

As shown in Table 1, the fundamental parameters used in the computational simulation of CZTS-based photovoltaic devices are provided [11–21]. The structure is arranged into layers, with the properties of the semiconductor material shaping the characteristics of the resulting structure.

The layer properties section provides thickness, electron affinity, relative permittivity, electron and hole mobilities, and donor and acceptor concentrations for the semiconductor layers (TCO, CdS, and CZTS), which govern the optoelectronic behaviour, including light absorption, charge-carrier generation, and transport.

In this section on the material properties of semiconductors, the focus is on the bandgap energy, effective densities of states in the conduction and valence bands, recombination velocities, defect density, and carrier capture cross-sections for the CZTS absorber layer. These parameters are essential for modelling the device performance. The parameters considered include bandgap energy (E_g), electron affinity (χ), dielectric permittivity (ε), conduction band density of states (N_c), valence band density of states (N_v), electron thermal velocity ($V_{\mathrm{th},n}$), hole thermal velocity ($V_{\mathrm{th},p}$), electron mobility (μ_n), hole mobility (μ_p), donor density (N_D), and acceptor density (N_A), as summarised in Table 1.

In conducting the simulation, the input parameters were either calculated or extracted from relevant literature. Additionally, all calculations were performed at a temperature of 300 K and under standard AM1.5 illumination.

This comprehensive set of material parameters serves as essential input for numerical simulations of CZTS-based solar cells, which are crucial for understanding device physics, optimising layer properties, and improving power conversion efficiency.

4. Results and Discussion

4.1. Optical properties

As demonstrated in Figure 3, the spectral photon flux of the product of effective albedo RA and the AM1.5G standard spectrum ($RA \times$ AM1.5G) is presented. The data presented herein were obtained using the MATLAB Simulink software to demonstrate the impact of varying the effective albedo (RA) on the back illumination received by a bifacial CZTS thin-film solar cell employed in the model. The effective albedo values range from 10% to 50%, with increments of 10% representing the fraction of incident sunlight reflected from the environment and subsequently available for rear-side absorption. The con-

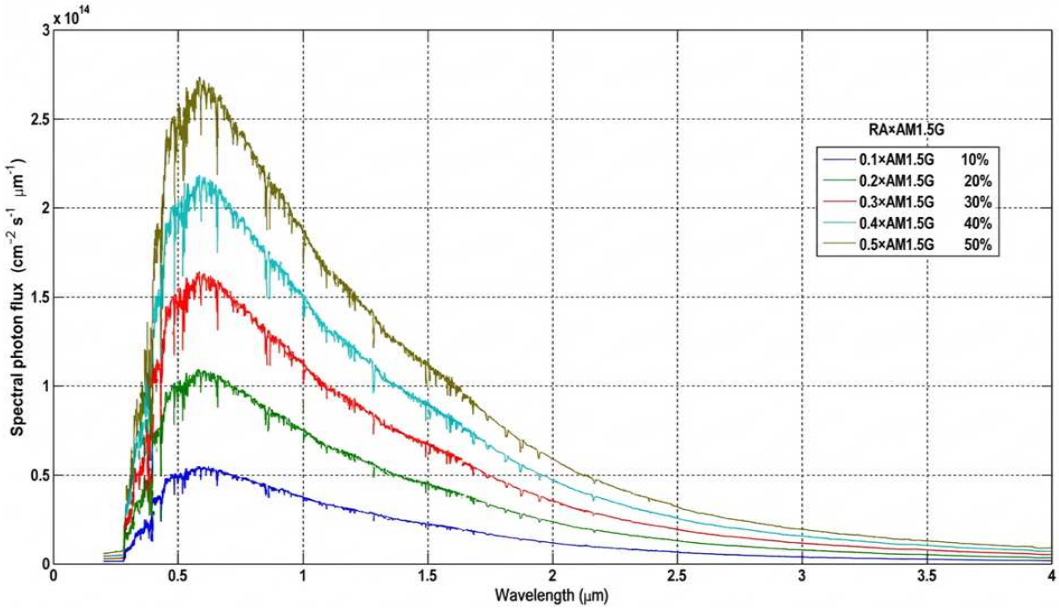

Fig. 3. Spectral irradiances of the RA × AM1.5G spectrum for the back illumination of the bifacial CZTS thin film solar cell

ditions have been meticulously designed to emulate the back-incident solar spectrum in realistic bifacial photovoltaic (PV) deployment scenarios with diverse surface reflectivities.

Each spectrum exhibits the characteristic shape of the AM1.5G profile, peaking near 0.5 μm in the visible region and gradually decreasing toward the infrared (IR). The uniformity of the albedo assumption across different RA levels indicates a spectral consistency in the albedo assumption, which is a valid simplification in first-order optical models. As RA increases, the spectral photon flux scales proportionally, with the peak photon flux reaching approximately 2.5×10^{14} cm^{-2} s^{-1} μm^{-1} at 50% albedo, compared to approximately 0.5×10^{14} cm^{-2} s^{-1} μm^{-1} at 10%. This linear scaling with RA underscores the direct and substantial influence of ground reflectivity on the rear-side photon availability in bifacial modules.

From a device design perspective, the presented spectra inform both optical and electrical modelling of bifacial CZTS thin-film solar cells. Accurate incorporation of backside illumination, especially in simulations predicting outdoor performance, is essential for performance forecasting and yield optimisation. Furthermore, the spectral peak aligns well with the optimal absorption range of CZTS (with a bandgap of approximately 1.5 eV), meaning that the additional photons introduced via reflection remain highly effective in generating charge carriers.

However, it is imperative to consider real-world factors such as the spectral selectivity of albedo, angular dependence of reflection, and partial shading. The assumption of isotropic and spectrally uniform albedo, while undoubtedly beneficial for theoretical exploration, may not fully capture the environmental complexities. Consequently, subsequent research endeavours should entail experimental validation employing bifacial thin-film CZTS modules operating under controlled albedo conditions, encompassing resolved albedo profiles for more comprehensive modelling. In essence, Figure 3 provides a clear demonstration that enhancing the effective albedo has a positive effect on the spectral photon flux incident on the rear side of bifacial CZTS thin-film solar cells, thus validating albedo engineering as a viable strategy for performance enhancement. It is vital to emphasise the significance of incorporating optical environment design into the development and deployment of next-generation bifacial photovoltaic technologies.

4.2. Impact of buffer and absorber variation on power conversion efficiency

Figure 4 demonstrates a monotonic decline in bifacial, front, and rear power conversion efficiency (PCE) as

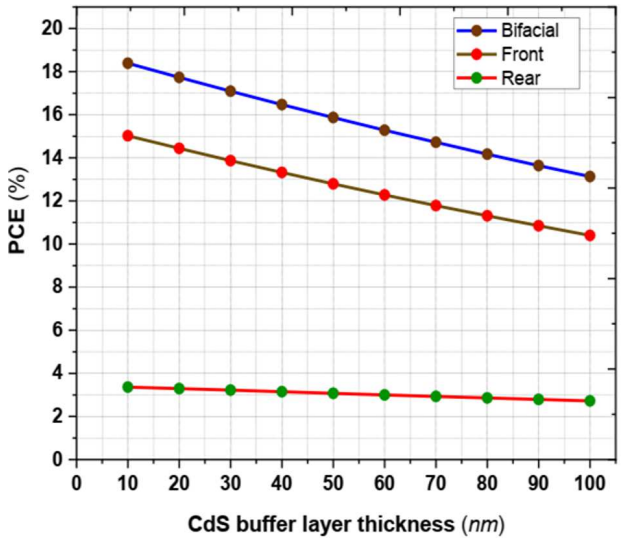

Fig. 4. Impact of CdS buffer layer thickness on PCE with CZTS fixed at 3 nm

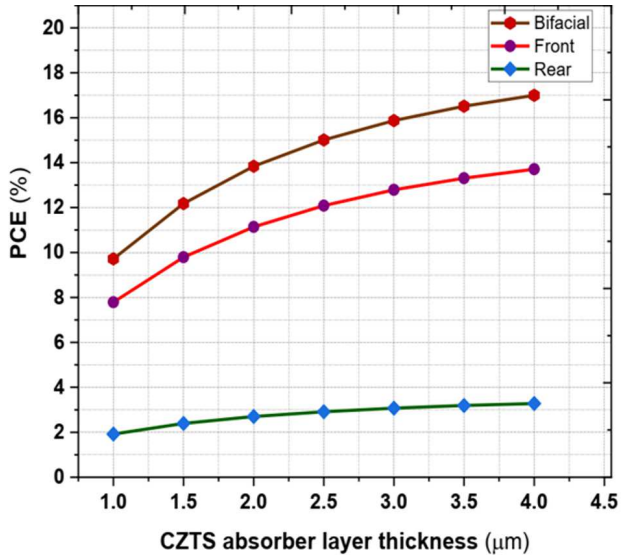

Fig. 5. Impact of absorber layer thickness on PCE with CdS fixed at 50 nm

the CdS buffer thickness increases from 10 to 100 nm for the CZTS absorber thickness fixed at 3 μm. The bifacial PCE decreases from 18.39% to 13.13%, indicating that the presence of thicker CdS results in significant net losses. The front-side PCE decreases by a similar margin (from 15.02% to 10.40%), confirming that the overall bifacial output is significantly influenced by front-side illumination.

This degradation is primarily attributed to enhanced parasitic absorption in the CdS buffer layer, which reduces the photon flux reaching the CZTS absorber. It is reasonable to hypothesise that additional electrical penalties arise from increased series resistance and longer carrier transport pathways through a thicker buffer layer. The rear-side PCE remains at a significantly lower level (decreasing from 3.36% to 2.72%) and exhibits weaker sensitivity to buffer thickness because the 3 μm CZTS absorber strongly attenuates incident light before it reaches the CdS layer.

The near-linear trends suggest that absorption-dominated losses prevail across the investigated thickness range rather than abrupt junction failure. It is therefore vital to minimise the CdS thickness within stable coverage limits to maximise the bifacial CZTS device performance.

Figure 5 demonstrates a systematic improvement in bifacial, front-side, and rear-side power conversion efficiency (PCE) with increasing CZTS absorber thickness when the CdS buffer layer is fixed at 50 nm. In accordance with the plotted trends, the bifacial PCE reaches its maximum at a CZTS thickness of 4 μm (17%) and declines to 9.72% at 1 μm, indicating that thinning of the CZTS absorber results in significant net efficiency losses. The front-side PCE exhibits a similar trend, decreasing from 13.71% at 4 μm to 7.79% at 1 μm, thereby confirming that the bifacial response is predominantly governed by front-side illumination performance.

The primary reason for this behaviour is reduced optical absorption in thinner CZTS layers, whereby a decreased absorber volume limits photon capture. Furthermore, thinner absorbers exacerbate interfacial and bulk recombination relative to the generated carrier population. The rear-side PCE remains lower overall, yet still decreases from 3.28% to 1.92% as the CZTS absorber is thinned, because rear-incident photons also require sufficient absorber thickness to be effectively harvested before recombination or transmission losses occur.

The uniformity of the curves indicates that the photogeneration and collection processes are constrained by absorber thickness rather than by exhibiting abrupt electrical degradation across the 1–4 μm range. Consequently, at a CdS thickness of 50 nm, it is imperative to maintain a sufficiently thick CZTS absorber layer (approximately 4 μm) to optimise bifacial device efficiency.

Figure 6 illustrates a consistent decline in bifacial, front, and rear power conversion efficiency (PCE) as the CdS buffer thickness increases from 10 to 100 nm at the CZTS absorber thickness corresponding to optimal performance (4 μm). The bifacial PCE decreases from 19.66% to 14.11%, indicating that the presence of thicker CdS results in significant net efficiency reductions. A similar trend is observed in the front-side PCE, which decreases from 16.07% to 11.19%, thereby confirming that bifacial output remains primarily influenced by front-side illumination collection.

This decline is primarily attributable to augmented parasitic absorption within the CdS buffer layer, which progressively filters short-wavelength photons and diminishes the generation rate in the CZTS absorber. It is also reasonable to hypothesise additional electrical penalties at larger buffer thicknesses, including higher series resistance and longer carrier transport paths across the buffer layer. The rear-side PCE remains considerably lower (decreasing from 3.59% to 2.91%) and exhibits weaker sensitivity to CdS thickness because rear-incident light is significantly attenuated as it traverses the thick CZTS absorber before reaching the CdS/CZTS junction.

The near-linear decline observed across all curves indicates that absorption-dominated losses prevail over the examined thickness range rather than that abrupt junction degradation. Consequently, it is vital to maintain a minimal CdS thickness within reliable coverage constraints to maximise the efficiency of bifacial CZTS devices at the optimal absorber thickness.

Figure 7 demonstrates a systematic enhancement in bifacial, front, and rear power conversion efficiency (PCE) with increasing CZTS absorber thickness when the CdS buffer layer is fixed at its optimal value of 10 nm. In alignment with the plotted trends, the bifacial PCE attains its maximum value at a CZTS thickness of 4 μm (19.66%) and subsequently diminishes to 11.36% at 1 μm, indicating that absorber thinning gives rise to substantial net efficiency losses. The front-side PCE displays an analogous dependence, decreasing from 16.04% at 4 μm to 9.25% at 1 μm, thereby confirming that bifacial performance remains predominantly driven by the front-side illumination response.

This behaviour is attributed to reduced optical harvesting in thinner CZTS layers due to insufficient absorber thickness, which limits photon absorption and carrier generation. Furthermore, the relative influence of bulk and interfacial recombination increases with thinner absorbers. The rear-side PCE is consistently lower but improves with absorber thickness, increasing from 2.11% at 1 μm to 3.59% at 4 μm. This improvement arises because a thicker CZTS layer is required to effectively capture rear-incident photons before transmission and recombination losses occur.

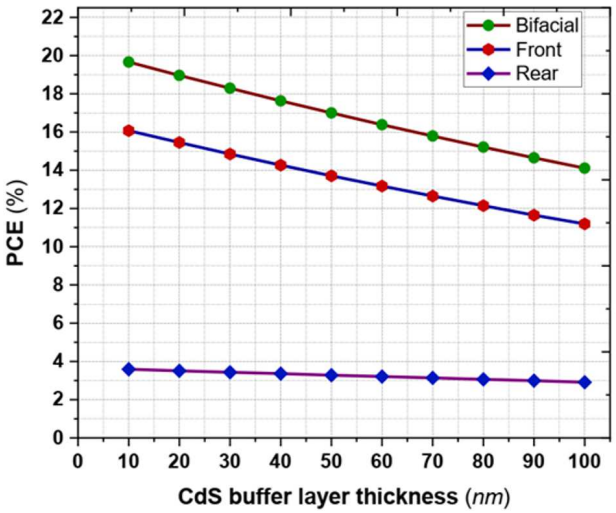

Fig. 6. Impact of CdS buffer layer thickness on PCE with CZTS fixed at 4 μm

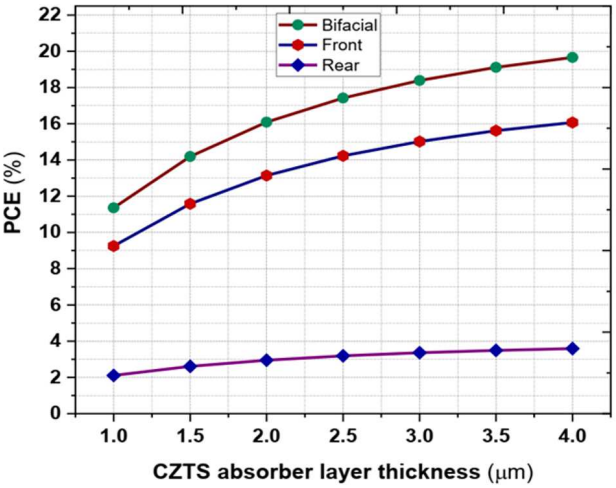

Fig. 7. Impact of CdS buffer layer thickness on PCE with CZTS fixed at 4 μm

The uniformity of the curves indicates that photogeneration and carrier collection are predominantly constrained by absorber thickness within the 1–4 μm range, rather than exhibiting abrupt electrical degradation. Consequently, to optimise bifacial device efficiency, it is imperative to maintain a relatively thick CZTS absorber (approximately 4 μm) when employing an optimal CdS buffer thickness of 10 nm.

5. Conclusion

This study aimed to compare and optimise monofacial and bifacial CZTS thin-film solar cells through numerical analysis. Using a self-consistent Poisson–drift–diffusion model implemented in MATLAB/Simulink, the research replaced the traditional opaque Mo back contact of the monofacial cell with a transparent conductive oxide, enabling dual-side photon harvesting. This modification provides a practical approach to boosting energy output in high-albedo environments. The results demonstrate that device performance is governed by a balance between optical absorption and recombination-limited carrier collection, with absorber and buffer layer thicknesses identified as the key determining factors.

Systematic parametric sweeps revealed that minimising parasitic absorption in the CdS buffer layer is essential for achieving optimal bifacial gain. Across both 3 μm and 4 μm absorbers, increasing the CdS thickness from 10 to 100 nm resulted in a nearly linear reduction in bifacial, front, and rear efficiencies. This behaviour indicates that optical filtering and transport losses rapidly outweigh any marginal junction advantages at larger buffer thicknesses. Conversely, increasing the CZTS absorber thickness from 1 to 4 μm consistently enhanced bifacial performance, suggesting improved photogeneration and more effective utilisation of rear-incident photons. The optimal configuration identified in this work, consisting of a 4 μm CZTS absorber combined with a 10 nm CdS buffer, achieved a peak simulated bifacial PCE of 19.66%, which is substantially higher than current experimental values ($\sim$12.6%) while remaining below the Shockley–Queisser theoretical limit for CZTS (32.4%).

These findings demonstrate that bifacial CZTS devices can achieve significant efficiency gains when optical losses at the buffer layer and rear interface are carefully minimised and when the absorber thickness is sufficient to enable dual-side photogeneration without excessive defect-related recombination. The remaining gap relative to the theoretical limit underscores the continued importance of defect density reduction, phase purity control, and rear-contact/interface optimisation. Accordingly, future research should incorporate experimentally validated, spectrally resolved albedo models and advanced recombination and defect-physics descriptions into numerical simulations, alongside proof-of-concept fabrication of bifacial CZTS device structures.

1. National Renewable Energy Laboratory (NREL) 2025, Best Research-Cell Efficiency Chart.
2. M.A. Green. Improved silicon optical parameters at 25 °C, 295 K and 300 K including temperature coefficients. Prog. Photovolt. *Res. Appl.* **30**, 164 (2021).
3. S. Suresh, D.J. Rokke, A.A. Drew, E. Alruqobah, R. Agrawal, A.R. Uhl. Extrinsic doping of ink-based Cu(In,Ga)(S,Se)2-absorbers for photovoltaic applications. *Adv. Energy Mater.* **12**, 2103961 (2022).
4. M. Minbashi, M.K. Omrani, N. Memarian, D. Kim. Comparison of theoretical and experimental results for band-gap-graded CZTSSe solar cell. *Curr. Appl. Phys.* **17**, 1238 (2017).
5. H.B. Sawa, M. Babucci, J. Keller, C.P. Björkman, N.R. Mlyuka, M.E. Samiji. Effects of Al_2O_3 rear interface passivation on the performance of bifacial kesterite-based solar cells with fluorine-doped tin dioxide back contact. *Phys. Status Solidi B* **261** (10), (2024)
6. W. Shockley, H.J. Queisser. Detailed balance limit of efficiency of *p–n* junction solar cells. *J. Appl. Phys.* **32**, 510 (1961).
7. W. Wang, M.T. Winkler, O. Gunawan, T. Gokmen, T.K. Todorov, Y. Zhu, D.B. Mitzi. Device characteristics of CZTSSe thin-film solar cells with 12.6% efficiency. *Adv. Energy Mater.* **4**, 1301465 (2013).
8. J. Kim, D. Kim, D. Hwang. Efficiency enhancement of bifacial $Cu_2ZnSnSe_4$ thin-film solar cells on indium tin oxide glass substrates by suppressing In–Sn diffusion with Mo interlayer. *J. Power Sources* **400**, 9 (2018).
9. M. Espindola-Rodriguez, D. Sylla, Y. Sánchez *et al.* Bifacial Kesterite Solar Cells on FTO Substrates.*ACS Sustain. Chem. Eng.* **5**, 11516 (2017).
10. D. Mora-Herrera, M. Pal, J. Santos-Cruz. Theoretical modelling and device structure engineering of kesterite solar cells to boost the conversion efficiency over 20%. *Sol. Energy* **220**, 316 (2021).
11. J. Kim, J. Kang, D. Hwang. Transparent conducting properties of Re-doped β-MoO_3 films. *APL Mater.* **4**, 096104 (2016).
12. S.M. Sze, M. Lee. *Semiconductor Devices: Physics and Technology* (Wiley, 2012).
13. J. Singh. *Optical Properties of Condensed Matter and Applications* (Wiley, 2006).

14. X. He, H. Shen, J. Pi, C. Zhang, Y. Hao, X. Shi. Synthesis and optical properties of Cu_2SnZnS_4 films under different sulfur atmospheres. *Rare Met.* **37**, 808 (2014).
15. F.Z. Boutebakh, A. Beloucif, M.S. Aida, A. Chettah, N. Attaf. Zinc molarity effect on Cu_2ZnSnS_4 thin film properties prepared by spray pyrolysis. *J. Mater. Sci.: Mater. Electron.* **29**, 4089 (2017).
16. A. Kanevce, I. Repins, S. Wei. Impact of bulk properties and local secondary phases on the Cu_2 (Zn, Sn) Se_4 solar cells open-circuit voltage. *Sol. Energy Mater. Sol. Cells* **133**, 119 (2014).
17. W. Zhang, C. You, Z. Dan, W. Wang, R. Dong. Improved performance of Cd-free CZTS thin-film solar cells by using $CZTS_{0.4}Se_{0.6}$ BSF layer. *J. Phys.: Conf. Ser.* **2418**, 012002 (2023).
18. W. Zhang, J. Tang, Y. Niu, R. Huang, L. Chen, M. Jiang. Study the best ratio of S and Se in CZTSSe solar cells with nontoxic buffer layer. *J. Renew. Sustain. Energy* **13**, 033501 (2021).
19. N.A. Benami. Effect of CZTS parameters on photovoltaic solar cell from numerical simulation. *J. Energy Power Eng.* **13**, 1 (2019).
20. O. Simya, A. Mahaboobbatcha, K. Balachander. A comparative study on the performance of Kesterite based thin film solar cells using SCAPS simulation program. *Superlattices Microstruct.* **82**, 248 (2015).
21. A. Emrani, P.P. Rajbhandari, T.P. Dhakal, C.R. Westgate. Cu_2ZnSnS_4 solar cells fabricated by short-term sulfurization of sputtered Sn/Zn/Cu precursors under an H_2S atmosphere. *Thin Solid Films* **577**, 62 (2015).

Received 30.12.25

М. Зебах, А. Хеммані, Х. Хачаб

ОПТИМІЗАЦІЯ ПРОДУКТИВНОСТІ ДВОБІЧНИХ ТОНКОПЛІВКОВИХ СОНЯЧНИХ ЕЛЕМЕНТІВ CZTS ДЛЯ ДОСЯГНЕННЯ МАКСИМАЛЬНОЇ ЕФЕКТИВНОСТІ ПЕРЕТВОРЕННЯ ЕНЕРГІЇ

Кестерит Cu_2ZnSnS_4 (CZTS) є одним з найперспективніших поглинальних матеріалів для тонкоплівкових сонячних елементів завдяки своєму прямозонному переходу (1,1–1,5 еВ), високому коефіцієнту поглинання ($>10^4$ см$^{-1}$), поширеності на Землі, нетоксичності та низькій вартості виробництва. Незважаючи на ці переваги, ефективність пристроїв на основі CZTS залишається обмеженою утворенням вторинної фази, електронними дефектами та нестабільністю виготовлення. У цій роботі розроблено числову модель для двобічного тонкоплівкового сонячного елемента CZTS з використанням самоузгодженого методу пуассонівського дрейфу-дифузії, реалізованої в MATLAB/Simulink. Шляхом оптимізації товщини поглинача та буферного шару досягнуто максимальної ефективності перетворення енергії (PCE) 19,66% для двобічного CZTS пристрою з поглиначем товщиною 4 мкм та буферним шаром CdS товщиною 10 нм. Цей результат перевищує зареєстровані експериментальні показники ефективності для подібних гетеропереходів CZTS (приблизно 15,8%), залишаючись при цьому нижчим за теоретичну межу Шоклі–Квайссера 32,4%. Отримані результати підкреслюють потенціал двобічних архітектур CZTS як ефективної стратегії покращення фотоелектричних характеристик сонячних елементів.

Ключові слова: сонячні елементи CZTS, тонкі плівки, двобічна фотоелектрична система, числове моделювання, гетероперехід.